SAND2000-3204J

SPATIAL BIAS IN FIELD-ESTIMATED UNSATURATED HYDRAULIC PROPERTIES

Robert M. Holt

Department of Geology and Geological Engineering, The University of Mississippi, University, Mississippi

John L. Wilson

Department of Earth and Environmental Sciences, New Mexico Institute of Mining and Technology, Socorro, New Mexico

Robert J. Glass

Geohydrology Department, Sandia National Laboratories, Albuquerque, New Mexico

DISCLAIMER

DISCLAIMER

ABSTRACT

Hydraulic property measurements often rely on non-linear inversion models whose errors vary between samples. In non-linear physical measurement systems, bias can be directly quantified and removed using calibration standards. In hydrologic systems, field calibration is often infeasible and bias must be quantified indirectly. We use a Monte Carlo error analysis to indirectly quantify spatial bias in the saturated hydraulic conductivity, K_s, and the exponential relative permeability parameter, α, estimated using a tension infiltrometer. Two types of observation error are considered, along with one inversion-model error resulting from poor contact between the instrument and the medium. Estimates of spatial statistics, including the mean, variance, and variogram-model parameters, show significant bias across a parameter space representative of poorly- to well-sorted silty sand to very coarse sand. When only observation errors are present, spatial statistics for both parameters are best estimated in materials with high hydraulic conductivity, like very coarse sand. When simple contact errors are included, the nature of the bias changes dramatically. Spatial statistics are poorly estimated, even in highly conductive materials. Conditions that permit accurate estimation of the statistics for one of the parameters prevent accurate estimation for the other; accurate regions for the two parameters do not overlap in parameter space. False cross-correlation between estimated parameters is created because estimates of K_s also depend on estimates of α and both parameters are estimated from the same data.

1.0 INTRODUCTION

In recent years, there has been an increased focus on characterizing the spatial variability of unsaturated hydraulic properties. Because laboratory methods for estimating unsaturated properties are expensive, time-consuming, and may not yield results representative of heterogeneous field conditions, simple and rapid field methods for estimating *in situ* unsaturated properties are appealing and potentially cost-effective. As a result, a variety of field methods for estimating *in situ* hydraulic properties have been developed (e.g., Reynolds and Elrick, 1985; Ankeny et al., 1991; Simunek and van Genuchten, 1996), and applied in spatial variability studies (e.g., Istok et al., 1994; Jarvis and Messing, 1995; Mohanty et al., 1994; Russo, et al., 1997; Shouse and Mohanty, 1998). Although most studies carefully document instrument procedures, little attention has been paid to examining hydraulic property measurement errors in the field. The absence of a rigorous treatment of property measurement errors in many of these studies is a potentially serious oversight, especially when hydraulic property data are used to characterize spatial variability.

Field measurement methods are often validated through limited testing in a known medium (e.g., Reynolds and Elrick, 1987; Simunek, et al., 1999) or by numerically simulating experimental results (e.g., Reynolds and Elrick, 1987; Simunek and van Genuchten, 1996; Wu, et al., 1997). In some cases, a cursory examination of errors has been performed (e.g., Simunek and van Genuchten, 1996; Russo et al., 1997). These types of validation can show that a method is useful for measuring *in situ* properties in the studied material. However, it is not sufficient for validating the use of a method in spatial variability studies where material properties vary over orders of magnitude. Measurements are only useful when they are sufficiently accurate for their intended purpose (e.g., Doebelin, 1966). Proper validation of a measurement technique for spatial variability studies should include systematic error analyses that considers the impact of measurement error on estimated spatial statistics, including the variogram. Without such a systematic evaluation, the reliability of data collected in spatial variability studies of unsaturated hydraulic properties remains suspect.

Errors in measured hydraulic properties are difficult to quantify. Most *in situ* hydraulic properties (e.g., hydraulic conductivity) are estimated indirectly using: 1) instruments that observe the response of a hydrologic system to a time-varying or steady boundary condition, and 2) non-linear mathematical-inversion models that infer property values from the observed responses. Because properties depend on non-linear inversion models, purely random error in the observation can lead to a systematic error, or bias, in the derived property value (Mandel, 1964). Bias may also result when the inversion model is inadequate (Kempthorne and Allmaras, 1986). We refer to these two contributions to measurement error as "observation error" and "inversion-model error", respectively.

Most texts on error analysis (e.g., Mandel, 1964, Doebelin, 1966) suggest that measurement bias can be experimentally evaluated and removed through the use of calibration standards. While individual components of an instrument may be calibrated, such as transducers used to observe response, the entire instrument including the inversion model must be calibrated to overcome the inversion non-linearity. Unfortunately, most instruments and methods for estimating *in situ* hydraulic properties are not directly calibrated because physical standards do not exist, and furthermore may never be calibrated because inversion-model errors vary unpredictably between individual field samples. In spatial variability studies, it is also impossible to fully calibrate estimates of the spatial statistics. Therefore, the effect of bias on spatial statistics cannot be directly quantified, and instead must be examined indirectly.

Measurement bias is potentially disastrous in the context of spatial variability studies. Because the observed response depends upon the hydraulic properties of the system, property measurement errors are correlated to the sampled hydraulic property. The spatial pattern of estimated hydraulic properties is distorted in space and estimated spatial statistics are also corrupted by bias and no longer representative. In summary, we hypothesize that field measurements of unsaturated hydraulic properties, and their spatial statistics, are spatially biased.

In this paper, we use a Monte Carlo error analysis to systematically evaluate for the first time the extent of bias in the spatial statistics of unsaturated hydraulic properties. Although the total inaccuracy of a measurement includes the effects of both bias and random errors (e.g., Mandel, 1964; Doebelin, 1966), bias is the most insidious component of error because it is difficult to identify or remove without calibration. Unsaturated property field instruments are seldom calibrated. We therefore focus on the issue of bias in this study. In particular, we consider tension-infiltrometer estimates of the saturated hydraulic conductivity and the pore-size distribution parameter for the exponential unsaturated hydraulic conductivity model. To keep our analysis tractable, we create an artificial reality in which the only errors affecting measurements are simple observation and inversion-model errors. This paper is not intended to be a detailed evaluation of all measurement error induced bias in spatial statistics tension-infiltrometer-estimated hydraulic properties. Instead, we focus on quantitatively revealing for the first time the impacts of measurement error bias on estimated spatial statistics. We do not consider sampling bias or uncertainty due to non-ideal sample locations or incomplete sampling.

2.0 METHODS

The tension infiltrometer is an instrument commonly used for examining the spatial variability of unsaturated hydraulic properties (e.g., DOE, 1993; Mohanty, et al., 1994; Jarvis and Messing, 1995; Shouse and Mohanty, 1998). It is a simple device for applying a constant (negative) pressure boundary condition to unsaturated soil (Figure 1). Contact with the soil is established using a porous membrane on the base-plate ring. Typically, a ring is placed on the soil surface and filled with fine sand. The base plate is placed upon the sand, which provides contact with the soil. Flow from the instrument is primarily caused by a capillary gradient. The flux from the instrument is determined by monitoring the declining water level in the Mariotte bottle (Figure 1). The design and operation of the tension infiltrometer is described by Ankeny et al. (1988).

A common inversion approach for the tension infiltrometer requires that the unsaturated hydraulic conductivity be described by an exponential relative permeability model, $\exp(\alpha\psi)$, where

$$K(\psi) = K_s \exp(-\alpha\psi), \tag{1}$$

ψ is the tension or the absolute value of the matric potential, α is the slope of $\ln[K(\psi)] / \psi$, and K_s is the saturated hydraulic conductivity. The exponential relative permeability model is commonly used in stochastic models of unsaturated flow (e.g., Yeh et al., 1985a, b, c; Mantoglou and Gelhar, 1987a, b; Polmann, et al., 1991; Indelman, et al., 1993; Russo, 1995; Harter and Yeh, 1996; Zhang et al., 1998). With knowledge of two applied tensions (ψ_1 and ψ_2) and corresponding observed steady-state flux rates (Q_1 and Q_2), parameters α and K_s can be estimated using the analytical approximation of Wooding (1968).

We employ a Monte Carlo approach to conduct our analysis. We generate 221 pairs of statistically homogeneous independent Gaussian random fields of $\ln(\alpha)$ and $\ln(K_s)$, with a zero specified point covariance between $\ln(\alpha)$ and $\ln(K_s)$. The pore-size parameter, α, is typically assumed to follow a normal distribution in most unsaturated stochastic models (e.g., Yeh et al., 1985a, 1985b, 1985c; Mantoglou and Gelhar, 1987a, 1987b; Indelman, et al., 1993; Zhang et al., 1998). However, we have chosen to describe α with a log-normal distribution because a log-normal distribution may be more realistic (e.g., White and Sulley, 1992; Russo et al., 1997). At each spatial location in a Monte Carlo simulation, we estimate the true flux and applied tension, add observation error to these values, and re-estimate $\ln(\alpha)$ and $\ln(K_s)$. To simplify our analysis, we assume that (1) describes the unsaturated hydraulic conductivity, Wooding's (1968) approximation is exact, and that sub-sample-scale heterogeneity (including macropores) does not exist. We consider only two types of observation error, error in estimated steady flux and error in applied tension, and only one type of model inversion error, error in contact between the disk and the medium. As in practice, we reject physically implausible results during the re-estimation. We examine biases affecting the mean, variance, and variogram model parameters for $\ln(\alpha)$ and $\ln(K_s)$ and define the parameter space in which these statistics can be predicted with minimal bias.

In this study, we do not consider the effects of structural errors, caused by a limited number of samples and non-ideal sampling locations, on variogram estimation. Most spatial variability studies are based on several hundred points or less, and structural errors introduce significant uncertainty in spatial statistics (e.g., Russo, 1984; Warrick and Myers, 1987; Russo et al., 1987a, b).

2.1 Random Fields ✓

For each Monte Carlo simulation we generate over 262,000 pairs (a 512 by 512 random field) of log-normal α and K_s with a fixed geometric mean and variance of α (α^G and $\sigma^2_{\ln(\alpha)}$) and K_s (K_s^G and $\sigma^2_{\ln(K_s)}$). The geometric means of α and K_s are varied between simulations. Philip (1969) suggests that the parameter α ranges between 0.002 to 0.05 cm^{-1}, although other reported values are both smaller than 0.002 cm^{-1} (e.g., Bresler, 1978; Russo and Bouton, 1992) and greater than 0.05 cm^{-1} (e.g., Clothier et al., 1985; Russo et al., 1997). α^G is varied from 10^{-4} to 0.1 cm^{-1} to encompass this range of values. Similarly, we vary K_s^G from 10^{-5} cm/s to 0.1 cm/s. This range is consistent with the range of hydraulic conductivity values reported in tension infiltrometer studies (e.g., Ankeny et al., 1991; Hussen and Warrick, 1993; Shouse and Mohanty, 1998) and is representative of silty sand to coarse sand (e.g., Freeze and Cherry, 1979). The variances of $\ln(\alpha)$ and $\ln(K_s)$ remain arbitrarily fixed at 1.0 which are consistent with the range of values reported from field studies (e.g., Russo and Bouton, 1992; Mohanty et al., 1994; Istok et al., 1994; Russo et al., 1997). Across our entire parameter space, we conduct 13 × 17 = 221 Monte Carlo simulations, in which the means of $\ln(K_s)$ and $\ln(\alpha)$ are each incremented by steps of size 0.576 between simulations.

In Richard's equation, the parameter α scales the influence of gravity (e.g., Philip, 1969). As α is increases, the slope of the $K(\psi)$ relationship increases indicating a narrowing of the pore-size distribution. By assuming that the pore-size distribution is proportional to the grain-size distribution, we can imply that the degree of sorting is inversely proportional to α. We can also infer that K_s increases with the average grain size. Across the parameter space the geometric mean values of α and K_s represent poorly to well-sorted silty sand to very coarse sand.

Random fields are generated using the FFT method (e.g., Robin et al., 1993). We employ a 2D, isotropic, exponential variogram model

$$\gamma^e(\mathbf{h}) = \sigma^2\left[1 - \exp\left(-\frac{\mathbf{h}}{\lambda_c}\right)\right] \tag{2}$$

where σ^2 is the variance of the random process, **h** is a separation vector, and λ_c is the correlation length. In stochastic models, it is often assumed that the correlation lengths of unsaturated parameters are the same (e.g., Yeh et al., 1985a, b, c; Mantoglou and Gelhar, 1987a, b) and, for convenience, we set all correlation lengths equal to 10 length units.

2.2 Observation Errors

Two sets of observations, each consisting of an applied tension and an observed steady-state flux, are required to estimate α and K_s. We assume that the applied tension is observed using a standard pressure transducer in the base plate (Figure 1). The flux from the Mariotte bottle is estimated by observing the height of water in the bottle with pressure transducers at two different times (e.g., Ankeny et al., 1988). Errors, in this case, are limited to transducer error and changes in tension due to bubbling within the Mariotte bottle.

The estimated tension, $\hat{\psi}$, at the base-plate membrane is expressed as

$$\hat{\psi} = \psi + \xi \tag{3}$$

where ψ is the true tension and ξ is the error due to transducer noise and drift and bubbling error. Because bubbling error is a time dependant phenomena, ξ has a temporal correlation. Ankeny et al. (1988) examined this issue and concluded that, in most cases, temporal correlation can be neglected. We assume that ξ is an independent, mean-zero, normally-distributed random variable and neglect transducer drift, implying that the transducers themselves are perfectly calibrated. With the assumption of independence, the variance of $\hat{\psi}$ is defined as

$$\sigma_{\hat{\psi}}^2 = \frac{\sigma_\xi^2}{M} \tag{4}$$

where σ_ξ^2 is the variance of ξ and M is the number of times the transducer is polled. Ankeny et al. (1988) reports that the standard deviation of observed pressure within their tension infiltrometer device is 0.62 cm. We assume that this variability is representative of the tension variation at the disk and set $\sigma_\xi^2 = 0.4\ \text{cm}^2$.

Estimates of the flux rate from a tension infiltrometer are most commonly based upon a method described by Ankeny, et al. (1988). Two transducers in the Mariotte tube are used to minimize, but not eliminate, the effect of bubbling errors. The flux rate, $\hat{Q}$, is estimated by determining the decline of water-level in the Mariotte tube as infiltration occurs and applying

$$\hat{Q} = \frac{\Delta \hat{H}}{\Delta t} \pi r_t^2 \tag{5}$$

where $\Delta \hat{H} = \hat{H}(t_2) - \hat{H}(t_1)$, $\Delta t = t_2 - t_1$ (the polling interval for the transducers), r_t is the radius of the Mariotte tube, and $\hat{H}(t)$ is the estimated height of the water in the Mariotte tube at time t. Flux errors are caused by errors in estimating the height of the water in the Mariotte tube,

$$\hat{H}(t) = H(t) + \varepsilon \tag{6}$$

where $H(t)$ is the true height of the water in the bubbling tube at time t and ε is an independent, mean-zero, normally-distributed error with variance σ_ε^2. As with the error in observed tension, the assumed distribution and assumption of independence of ε is an approximation that improves when the sampling period is much greater than the bubble frequency. If N flux estimates are averaged, then the variance of this estimate is

$$\sigma_q^2 = \frac{2\sigma_\varepsilon^2 \pi^2 r_t^4}{\Delta t^2 N} \tag{7}$$

We estimate $\sigma_\varepsilon^2 = 0.0025\,\text{cm}^2$ from the results of Figure 2 of Ankeny et al. (1988), with spurious data removed. We also assume that the radius of the bubbling tube r_t is 1 cm, that the pressure transducer is polled once per second, and 30 seconds worth of data are averaged to estimate the steady-state flux rate. Using (7), the variance of estimated flux rates is $\sigma_q^2 = 0.00165\ \text{cm}^6/\text{s}^2$.

2.3 Contact Error

We consider only one type of inversion-model error, a "contact error" resulting from poor contact between the base-plate membrane and the sample medium. It is a common problem during use of the tension infiltrometer and, in our experience, appears to occur more frequently for observations made at higher tensions. This type of error reduces the area for flow and alters the flow geometry. Flaws in the sand contact between the disk and the medium act as large pores, which do not fill at high tensions. At lower tensions, these pores fill eliminating or reducing the error. Since the tension infiltrometer requires at least two observations, one at a higher tension, this error is often more pronounced at the higher tension.

We are not interested in studying contact error in detail, but only its impact on estimating spatial statistics. Consequently, we develop and apply a simple approximation based upon the reduction of area for flow. We assume that the flow geometry does not change and that only the disk area is reduced due to poor contact. We apply this error only at the highest applied tension. The disk area is multiplied by a scaling factor $(1-f)$, where f is selected from a uniform random distribution over 0.0 to 0.1. Because estimates of α and K_s require two flux observations, this error introduces an additional bias in the estimated hydraulic properties. In the following sections, the contact error scenario includes both the contact and observation errors.

2.4 Hydraulic Property Estimates

We assume that the tension values used for each observation are estimated to be $\hat{\psi}_1 = 2.0$ cm and $\hat{\psi}_2 = 7.0$ cm. The true tensions (ψ_n) are calculated by subtracting ξ from $\hat{\psi}_n$, for $n = 1,2$. For each observation, the value of ξ is determined by randomly sampling a mean-zero normal distribution with $\sigma_\xi^2 = 0.4$ cm^2. Given ψ_n, α, and K_s, we calculate the true flux from the tension infiltrometer using (Wooding, 1968)

$$Q_n = \frac{K_s}{\alpha} e^{-\alpha \psi_n} \left(\alpha + \frac{4}{\pi r_d} \right) \pi r_d^2 \tag{8}$$

where r_d is the radius of the disk and is equal to 10 cm.

Once the true flux rate is determined, we calculate the estimated flux $\hat{Q}_n$ by adding mean-zero, normally distributed error with $\sigma_q^2 = 0.00165$ cm^4/s^2. Sampling locations where $\hat{Q}_1 \leq \hat{Q}_2$ are discarded, as they would be in practice. Although we and others (e.g., Mohanty, pers. comm., 2000; Ankeny, pers. comm., 2000) have both observed and followed this practice in field studies, it is not well documented in the literature. The percentage of discarded points is usually small. For our field studies it is typically around 5%.

When contact errors are considered, $\hat{Q}_1$ is estimated using the procedure outlined above, while $\hat{Q}_2$ is estimated using the same variance for σ_q^2 but is estimated using an altered disk radius

$$r_d^* = r_d\sqrt{1-f} \tag{9}$$

where f is sampled from a uniform distribution over 0.0 to 0.1. This means that the disk radius may be reduced from 10 cm to a minimum of ~ 9.5 cm.

The relative permeability parameter, α, is then estimated with (Reynolds and Elrick, 1991)

$$\hat{\alpha} = \frac{\ln(\hat{Q}_1/\hat{Q}_2)}{\hat{\psi}_2 - \hat{\psi}_1} \tag{10}$$

and the saturated hydraulic conductivity, K_s, is estimated with

$$\hat{K}_s = \frac{\hat{\alpha}\ \hat{Q}_1 e^{\hat{\alpha}\hat{\psi}_1}}{\hat{\alpha}\pi r_d^2 + 4r_d} \tag{11}$$

This procedure is repeated for all pairs of α and K_s values.

2.5 Statistical Property Estimates

For each spatially correlated random field, the mean, variance, and cross-covariance between $\ln(\alpha)$ and $\ln(K_s)$ are determined. In addition, local variograms are calculated for $\ln(\alpha)$, $\ln(K_s)$, $\ln(\hat{\alpha})$, and $\ln(\hat{K}_s)$ using the GSLIB subroutines gam2 (Deutsch and Journel, 1998)

$$\gamma(\mathbf{h}) = \frac{1}{2N(\mathbf{h})}\sum_{i=1}^{N(\mathbf{h})}\left[U(\mathbf{x}_i+\mathbf{h}) - U(\mathbf{x}_i)\right]^2 \tag{12}$$

where N(**h**) is the number of samples in lag interval **h** and U(x) is the random field. All of the resulting 221 experimental variograms are fit using a Levenberg-Marquardt algorithm with the exponential variogram model

$$\hat{\gamma}^{m}(\mathbf{h}) = \sigma_{m}^{2}\left[1-\exp\left(-\frac{3\mathbf{h}}{\hat{\lambda}_{c}}\right)\right]+\sigma_{n}^{2} \tag{13}$$

where $\hat{\lambda}_c$ is the estimated "correlation length", $\hat{\sigma}_m^2$ is the "model variance", and $\hat{\sigma}_n^2$ is the nugget variance. The variance is equal to the sum of the model and nugget variances. When a variogram is constant for all lag distances, we refer to it as a "nugget variogram" in which $\hat{\sigma}_m^2 = 0.0$ and $\hat{\lambda}_c = 0.0$. In classical geostatistics, nugget variograms represent white noise processes that have no spatial correlation. Bias for each statistical parameter is shown using a ratio

$$\hat{P}_E / \hat{P}_T \tag{14}$$

where $\hat{P}_E$ is the statistical parameter (e.g., mean, variance, or variogram model parameters) for a random field of estimates and $\hat{P}_T$ is the statistical parameter determined for the true random field. The ratio equals 1.0 for an unbiased statistic.

3.0 RESULTS

Here, we present the results of our Monte Carlo analysis. We show that both the fraction of points discarded because of a physically implausible result ($\hat{Q}_1 \leq \hat{Q}_2$), and the bias in the mean, variance, and variogram-model parameters for $\ln(\hat{\alpha})$ and $\ln(\hat{K}_s)$, are functions of the field values of K_s^G and α^G. In addition, we illustrate how measurement errors introduce false cross-correlation between $\ln(\hat{\alpha})$ and $\ln(\hat{K}_s)$. When only measurement errors are considered, bias in spatial statistics increases for those geometric mean values that produce low flux rates (e.g., small K_s and high α) and appears to correlate with the fraction of points discarded. When inversion-model errors, in the form of a contact error, are included, the pattern of bias in spatial statistics changes significantly and depends less on the fraction of points discarded.

3.1 Fraction of Points Discarded

Figures 2a and 2b plots across parameter space the fraction of points discarded (FPD) because of an unrealistic result, $\hat{Q}_1 \le \hat{Q}_2$. When only observation errors are considered (Figure 2a), the FPD is a function of both K_s^G and α^G. The FPD increases with α^G and decreases with K_s^G. This result is not surprising, because relative errors in flux rates increase when the flux rates are small and small flux rates result from high α and small K_s (8). In the upper left corner (high α^G and small K_s^G), estimated fluxes $\hat{Q}_1$ and $\hat{Q}_2$ are dominated by errors and are nearly independent of the sampled values of α and K_s. In these regions, the likelihood that $\hat{Q}_1 \le \hat{Q}_2$ is high, and the FPD increases. When contact error is included (Figure 2b), the FPD tends to become less dependent on the value of K_s at low α^G, and the FPD decreases across much of the parameter space. This occurs because contact error tends to decrease $\hat{Q}_2$, reducing the likelihood that $\hat{Q}_1 \le \hat{Q}_2$.

3.2 Bias in Estimated Mean

Figure 3a presents the bias, expressed as a ratio, in the geometric mean of $\hat{\alpha}$, or $\hat{\alpha}^G$, across parameter space. As the field value of either α^G or K_s^G decreases (lower left portion of parameter space), the amount of bias in $\hat{\alpha}^G$ increases significantly to over five times the true value. It is not surprising that bias would increase at small K_s^G, because $\hat{Q}_1$ tends to be overestimated and $\hat{Q}_2$ tends to be underestimated as the FPD increases. However, it seems contradictory that bias is less at high α^G, because the FPD increases there. This occurs because bias in the log flux ratio, $\ln\left(\hat{Q}_1/\hat{Q}_2\right)$ from (10) differs from bias in the flux rates themselves, $\hat{Q}_1$ and $\hat{Q}_2$. At a small α^G, flux-rate errors are relatively small, but errors in the log ratio are very large. Therefore, relatively small errors in flux-rates cause large, positively biased errors in the flux ratio and $\hat{\alpha}$.

The bias in the geometric mean of the estimated K_s, or $\hat{K}_s^G$, is shown in Figure 3c and is similar to the bias in $\hat{\alpha}^G$, except that it is less sensitive to α^G. The parameter $\hat{K}_s$ is a linear function of $\hat{Q}_1$ (11), and, as K_s^G decreases, $\hat{Q}_1$ is overestimated because the FPD increases. Therefore, bias in $\hat{K}_s^G$ is nearly independent of α^G.

Figures 3b and 3d show that the bias in $\hat{\alpha}^G$ and $\hat{K}_s^G$ changes drastically when contact error is added. $\hat{\alpha}^G$ is only accurately estimated in a narrow region at high α^G, near the top of parameter space, while $\hat{K}_s^G$ is overestimated across the entire parameter space. There is much less dependence on K_s^G, and the bias is much greater at low α^G. The contact errors decrease $\hat{Q}_2$, leading to an increase in the flux ratio and overestimation of $\hat{\alpha}$ and $\hat{K}_s$. For low α's the biased estimates, $\hat{\alpha}^G$ and $\hat{K}_s^G$, are both well over an order of magnitude too high.

3.3 Bias in Estimated Variance

Bias in the variance of $\ln(\hat{\alpha})$ is depicted across parameter space in Figure 4a. The bias increases as α^G and K_s^G decreases (lower left corner of parameter space), except at very small K_s^G (far left portion of parameter space) where the bias decreases again. As α^G or K_s^G decreases, the variability of the log ratio in (10) increases, causing the variance of $\ln(\hat{\alpha})$ to increase. At very small K_s^G, however, $\hat{Q}_1$ and $\hat{Q}_2$ are dominated by errors and are independent of sampled α and K_s. The variability of the log ratio is reduced, and the variance of $\ln(\hat{\alpha})$ decreases.

Figure 4b illustrates bias in the variance of $\ln(\hat{\alpha})$ when contact errors are added. There is much less dependence on the K_s^G, and the variance of $\ln(\hat{\alpha})$ is underestimated at large K_s^G. In this case, $\hat{Q}_2$ tends to underestimate Q_2 because the disk area is reduced. The log ratio in (10) is consistently overestimated, and the amount of overestimation increases at low α^G where the true flux ratio is small. This effect is most pronounced for higher K_s^G, where $\hat{Q}_1$ and $\hat{Q}_2$ are strongly dependent upon the values of K_s and α. The variability of the log ratio and the variance of $\ln(\hat{\alpha})$ decreases. Contact effects decrease as K_s^G decreases, because both $\hat{Q}_1$ and $\hat{Q}_2$ become increasingly independent of α and K_s (i.e. independent of Q_1 and Q_2).

Figure 4c shows bias in the variance of $\ln(\hat{K}_s)$. Bias increases at high α^G and small K_s^G. Recalling that $\hat{K}_s$ is a function of both $\hat{\alpha}$ and $\hat{Q}_1$, this relationship appears counter-intuitive, because the variance of $\ln(\hat{\alpha})$ decreases as α increases and the variability of $\hat{Q}_1$ decreases at high α^G and low K_s^G. Compensating effects, however, cause the observed behavior. Consider the covariance between $\hat{Q}_1$ and $\hat{\alpha}$ in

$$\mathrm{var}\left[\ln(\hat{K}_s)\right] \propto \mathrm{var}\left[\ln(\hat{\alpha})\right] + \mathrm{var}\left[\ln(\hat{Q}_1)\right] + 2\,\mathrm{cov}\left[\ln(\hat{\alpha}), \ln(\hat{Q}_1)\right] \tag{15}$$

In general, estimated $\ln\left(\hat{Q}_1\right)$ and $\ln(\hat{\alpha})$ exhibit a large negative covariance, except for that portion of our parameter space where the fluxes become independent of α and K_s. Independence occurs at high α^G or small K_s^G, where more points are discarded (Figure 2). Here the negative covariance between $\ln(\hat{\alpha})$ and $\ln(\hat{Q}_1)$ approaches zero faster than the positive variances of $\ln(\hat{\alpha})$ and $\ln(\hat{Q}_1)$ decrease. Therefore, the variance of $\ln(\hat{K}_s)$ increases for high α^G or small K_s^G.

The bias in the variance of $\ln(\hat{K}_s)$ changes significantly when contact errors are present (Figure 4d), as overestimation increases. At high K_s^G, the bias is nearly independent of K_s^G and increases dramatically as α^G decreases. When contact errors are present, $\hat{\alpha}$ tends to be overestimated leading to overestimation of $\hat{K}_s$ (Figures 3c and 3d). This effect is most pronounced in parameter space where the flux rates are strongly dependent on α and K_s, that is in the lower right corner of the parameter space where K_s^G is large and α^G is small. In this region, $\hat{\alpha}$ depends primarily on the errors in the estimate of $\hat{Q}_2$, and the correlation between $\hat{Q}_1$ and $\hat{\alpha}$ decreases. Consequently, the variance of $\ln(\hat{K}_s)$ tends to increase (15).

3.4 Bias in Variograms

Bias in the variogram model variance and correlation length for $\ln(\hat{\alpha})$ are shown in Figures 5a and 5b, respectively. The model variance is mostly overestimated, while the correlation length is underestimated. The pattern of error in the model variance is similar to the pattern of error in the variance of $\ln(\hat{\alpha})$ (Figure 4a), except in the upper left corner of parameter space (high α^G and small K_s^G) where the model variance approaches zero. Correlation lengths are accurately estimated, with bias values near one, across most of the parameter space. As with the model variance, correlation lengths become inaccurate in the upper left corner of parameter space (Figure 5b), with a bias ratio approaching zero. Correlation lengths and model variances approach zero as estimates of the flux rates become dominated by errors, rather than the true values of α and K_s. At low α^G and small K_s^G, flux-rate errors greatly increase the variance of $\ln(\hat{\alpha})$ (Figure 4a), but do not disrupt estimation of spatial correlation, because bias in the flux-rates accentuates spatial differences of $\ln(\hat{\alpha})$.

Figures 5c and 5d display the bias in the model variance and correlation length for $\ln(\hat{\alpha})$ when contact errors are added. Both are underestimated. The underestimation is significant at high α^G and small K_s^G and across a broad region characterized by low α^G. In the upper left corner of parameter space where α^G is high and K_s^G is small, as with the case with no contact error (Figures 5a and 5b), flux rates are dominated by errors, and $\ln(\hat{\alpha})$ loses spatial correlation. However, along the bottom of the figure, with low α^G, estimates of $\hat{Q}_2$ are too small leading to consistent overestimation of $\ln(\hat{\alpha})$ and a reduction of spatial correlation. The spatial statistics are those of a nugget.

Figures 6a and 6b present the bias in the model variance and correlation length for $\ln(\hat{K}_s)$. Model variances and correlation lengths are accurately estimated across most of the parameter space, but greatly underestimated at small K_s^G, especially in combination with a low α^G. The variogram of $\ln(\hat{K}_s)$ is proportional to $\gamma_{\ln(\hat{\alpha})} + \gamma_{\ln(\hat{Q}_1)} + 2\gamma_{\ln(\hat{\alpha}),\ln(\hat{Q}_1)}$, where $\gamma_{\ln(\hat{\alpha})}$ is the variogram of $\ln(\hat{\alpha})$, $\gamma_{\ln(\hat{Q}_1)}$ is the variogram of $\ln(\hat{Q}_1)$, and $\gamma_{\ln(\hat{\alpha}),\ln(\hat{Q}_1)}$ is the cross-variogram between $\ln(\hat{\alpha})$ and $\ln(\hat{Q}_1)$. This relationship is primarily responsible for the patterns displayed by errors in the model variance and correlation length. Of particular importance is $\gamma_{\ln(\hat{\alpha}),\ln(\hat{Q}_1)}$, which tends to reduce the variogram of $\ln(\hat{K}_s)$ because $\ln(\hat{\alpha})$ and $\ln(\hat{Q}_1)$ are negatively correlated. At high α^G and small K_s^G (upper left corner), flux rates are dominated by errors, and $\gamma_{\ln(\hat{\alpha})}$, $\gamma_{\ln(\hat{Q}_1)}$, and $\gamma_{\ln(\hat{\alpha}),\ln(\hat{Q}_1)}$ have little correlated spatial structure. Consequently, the model variance and correlation length of $\ln(\hat{K}_s)$ are reduced in this region. At low α^G, however, spatial structure is preserved in $\gamma_{\ln(\hat{\alpha})}$, $\gamma_{\ln(\hat{Q}_1)}$, and $\gamma_{\ln(\hat{\alpha}),\ln(\hat{Q}_1)}$, but the negative correlation between $\ln(\hat{\alpha})$ and $\ln(\hat{Q}_1)$ is strong, and little spatial structure is preserved in the variogram of $\ln(\hat{K}_s)$. At low α^G and small K_s^G (lower left corner), $\ln(\hat{\alpha})$ is dominated by errors in $\hat{Q}_1$, as $\hat{Q}_1$

tends to have more error than $\hat{Q}_2$, and the magnitude of the cross-covariance between $\ln(\hat{\alpha})$ and $\ln(\hat{Q}_1)$ increases.

When contact error is added, patterns of bias in the model variance and correlation length of $\ln(\hat{K}_s)$ change (Figures 6c and 6d). Similar to errors in the variance of $\ln(\hat{K}_s)$ (Figure 4d), model variance bias increases significantly at low α^G. Errors in the cross-variogram between $\ln(\hat{\alpha})$ and $\ln(\hat{Q}_1)$ still strongly control the variogram of $\ln(\hat{K}_s)$. At low α^G, $\ln(\hat{\alpha})$ is controlled by errors in $\hat{Q}_2$, and $\gamma_{\ln(\hat{\alpha}),\ln(\hat{Q}_1)}$ is small. As a result, the estimated correlation length of $\ln(\hat{K}_s)$ is fairly accurate (Figure 6d), but the model variance is greatly overestimated (Figure 6c). As with the case with no contact error, model variances and correlation lengths approach zero at high α^G and small K_s^G (upper left corner), because flux rate estimates are dominated by errors.

3.5 Cross-Correlation

Although true properties $\ln(\alpha)$ and $\ln(K_s)$ are statistically independent, we observe significant cross-correlation between estimated properties $\ln(\hat{\alpha})$ and $\ln(\hat{K}_s)$ (Figure 7). False cross-correlation between $\ln(\hat{\alpha})$ and $\ln(\hat{K}_s)$ results because both $\hat{\alpha}$ and $\hat{K}_s$ depend on $\hat{Q}_1$ (10 and 11), and $\hat{K}_s$ depends on and increases with $\hat{\alpha}$ (11), yielding positive point correlation functions. When only measurement errors are present, the correlation coefficient for $\ln(\hat{\alpha})$ and $\ln(\hat{K}_s)$ appears to increase as K_s^G decreases, reflecting increasing errors in the flux rates. When contact errors are also present, the pattern of the correlation coefficient changes, and strong cross-correlation is observed at both large K_s^G and low α^G (lower right corner), and small K_s^G and high α^G (upper left corner of parameter space). This occurs because $\hat{\alpha}$ tends to be overestimated in this region of parameter space (Figure 3b).

With the tension infiltrometer we use one parameter ($\hat{\alpha}$) to estimate another ($\hat{K}_s$). Errors in the first parameter generate errors in the second, resulting in apparent cross-correlation. Similar cross-correlation can occur if a single data set is used to estimate multiple parameters, because errors in the data set will propagate through multiple inversions. Cross-correlation due to measurement error may enhance or obscure the true cross-correlation between hydraulic parameters.

4.0 DISCUSSION

In this paper, we focus on revealing some of the impacts of tension infiltrometer measurement error on estimated spatial statistics. In the following discussion, we argue that our results are over optimistic for many applied field situations. We first show that observation errors are likely to be much greater than those used in this study. We have also neglected a large number of inversion-model errors that can cause spatial bias. We then discuss the implications this work for tension infiltrometer field studies. Finally, we illuminate the general problem of bias in hydrologic property measurements.

4.1 Range of Observation Errors

In most field studies, observation errors are likely to be greater than those used for this study. The flux-rate errors used here were based on instrument observations reported by Ankeny et al. (1988). Because their observations were made under highly controlled laboratory conditions (Ankeny, pers. com., 1998), we conducted a series of laboratory repeatability studies to directly evaluate the flux-rate variance, σ_q^2, during realistic tension infiltrometer operation. A large sandbox was constructed and filled with well-sorted, fine sand. The tension infiltrometer (manufactured by Soil Measurement Systems of Tucson, Arizona) was calibrated using standard methods (e.g., Soil Measurement Systems, 1992), and applied following normal procedures. After each test, the sand was returned to a constant initial condition by applying a vacuum to a pressure plate at the base of the box. For these tests, σ_q^2 was determined to be 0.06 cm^6/s^2. This value may be a more representative more representative of field studies than the flux-error variance used here ($\sigma_q^2 = 0.00165$ cm^6/s^2).

Errors in applied tension at the disk source may also be much larger than considered here. Many tension infiltrometers do not have a pressure transducer located at the disk source. Instead the applied tension at the disk is traditionally calibrated at a given bubble rate (e.g., Soil Measurement Systems, 1992). A constant bubble rate is achieved by establishing a vacuum on the Mariotte bottle, and a manometer is connected to the source tube for the disk. The depth of the air entry tubes is adjusted until the desired tension in the source tube is reached. This approach, however, is subject to a variety of errors. Because temperature changes will affect the expansion of bubbles, effective steady-state tensions will systematically vary from the calibrated values. In addition, some tension infiltrometers have a separate disk, and errors will be introduced if the disk is not at the correct elevation relative to the Mariotte bottle.

4.2 Neglected Inversion-Model Errors

Infiltrometer operators generally try to minimize observation errors by calibrating some of the components of infiltrometer and changing the diameter of the Mariotte bottle (Ankeny et al., 1988). In principle, bias due to observation errors can be significantly reduced by virtually eliminating these errors, provided that the inversion model is not too non-linear. Changing the inversion model can also reduce bias due to inversion-model error. Because it is virtually impossible to completely and accurately incorporate all of the physics relevant to a hydraulic property measurements at every sampled location (Beckie, 1996), it is unlikely an inversion model can be found that is completely free of error. As our results show, a simple inversion-model error, contact between the disk source and the sampled medium, can lead to large amounts of spatial bias. A variety of other types of inversion-model error could cause a different, yet still significant, bias in spatial statistics.

Consider the effects of viscosity errors due to temperature changes. Standard inversion models for the tension infiltrometer assume that the viscosity of the infiltrating water remains constant (e.g., Ankeny, 1991; Reynolds and Elrick; 1991). This is very unlikely, especially in the field where the temperature of water in the infiltrometer will almost certainly be different from the soil temperature. A temperature drop of 1° C will result in an increase in the viscosity of pure water of ~2% (Weast, 1972), resulting in a ~2% decrease in unsaturated hydraulic conductivity. This change could cause significant bias in properties estimated with the tension infiltrometer.

In a field situation, bias due to viscosity errors would be temporal. In the morning, the water temperature in the infiltrometer could be greater than that of the soil and soil water. Infiltrating water would cooler during the measurement of $\hat{Q}_2$ and warmer during the measurement of $\hat{Q}_1$. These differences would lead to a smaller FPD and an overestimation of the flux ratio, $\hat{\alpha}$, and $\hat{K}_s$. In the afternoon, the situation could be reversed. In this situation, the temporal bias due to viscosity errors would appear as noise that may cause underestimation of the model variance and the correlation length.

A variety of other inversion-model errors will also produce bias that affects spatial statistics. Other potential sources of bias include sub-sample-scale heterogeneity, changes in the medium due to infiltration, soils with non-exponential hydraulic conductivity functions, and air entrapment. As with our contact error, many of these errors could cause significant bias in estimated spatial statistics, and their impact should be studied.

4.3 Implications for Tension Infiltrometer Studies

Our results indicate that tension infiltrometer observation and contact errors will lead to overestimation of both $\hat{\alpha}$ and $\hat{K}_s$. This is consistent with Ankeny et al. (1991), who observed that on average tension infiltrometer measurements of $\hat{K}_s$ overestimate laboratory measurements by a factor of 3. The mathematical character of tension infiltrometer inversion models leads to overestimation of $\hat{\alpha}$ and $\hat{K}_s$ in the presence of observation errors. Data with $\hat{Q}_1 \leq \hat{Q}_2$ are rejected because they yield an unreasonable result, that is negative values of $\hat{\alpha}$. A large FPD is therefore an indicator of potential bias in tension infiltrometer results.

It is important to recognize, however, that a small FPD does not necessarily imply a small spatial bias. Three possible explanations can account for a small FPD in field studies. Measurement errors could be very small, the mean value of the sampled K_s could be large and the mean α could be small, or inversion-model errors could reduce the FPD. Recall that our contact error reduces the FPD across parameter space, yet causes much more bias in spatial statistics than observation errors. Other inversion-model errors, including viscosity errors, could cause a similar effect.

Our results also indicate that measurement errors can introduce false cross-correlation between $\hat{\alpha}$ and $\hat{K}_s$. Because $\hat{K}_s$ is proportional to $\hat{\alpha}$, correlation coefficients will show a positive bias, and very large positive correlation coefficients are a possible indicator of error. Negative correlation coefficients, however, do not indicate the absence of measurement error bias.

The other spatial statistics (mean, variance, and variogram) offer few diagnostic indicators of measurement bias. In fact, spatial statistics can appear realistic, but still be strongly biased. Nugget variograms could indicate either strong bias or lack of spatial correlation. Similarly a nugget effect in the variogram, a positive difference between the variance and model variance, could indicate bias but may also indicate uncorrelated random errors, sub-sample scale heterogeneity, or non-ideal sample location (e.g., Journel and Huijbregts, 1978).

Unfortunately, we find no unique indicators of bias in tension infiltrometer data. Certain results (e.g., large FPD, large positive correlation coefficients, and nugget variograms) can strongly suggest the presence of bias, but indicators of little or no bias are not obvious from our results. Investigators should take care to minimize observation errors, thereby reducing observation error bias. In addition, workers should diligently attempt to identify, quantify, and treat, possibly with error analyses, inversion-model errors that are likely to affect their measurements. Finally, spatial statistics should be considered with skepticism unless they are validated through an error analysis or independent metric.

4.4 The Bias Problem

Bias in property measurements is a critical problem in groundwater hydrology that potentially affects many hydraulic property measurements. For most measurement systems in physics and engineering, calibration is used to quantify and remove measurement bias (e.g., Mandel, 1964; Doebelin, 1966). Although the individual components of many devices used for measuring hydraulic properties are calibrated (e.g., Ankeny, 1988), calibration of device components does not insure the elimination of measurement bias. Unbiased errors in the device response can still lead to bias in measurements that use a non-linear inversion model (e.g., Mandel, 1964). Calibration standards are available and incorporated into some field hydraulic property measurement procedures (e.g., Davis, et al., 1994). Using calibration standards, bias can be effectively quantified and eliminated from measured hydraulic properties only when the physical processes, including process time and length scales, in the standard and the sample are similar.

For many field methods used to estimate porous media hydraulic properties, like the tension infiltrometer, whole instrument field calibration standards are not feasible or practical, and the exact nature of the bias induced by property-measurement errors cannot be directly quantified or removed. For these methods, bias can only be quantified using indirect approaches such as a Monte Carlo error analysis. Given the wide range of types of error that may affect measurements of properties, however, it may be impossible to identify and model their effects for every property estimation technique.

5.0 Summary and Concluding Remarks

In this paper, we show that small observation and inversion-model errors bias unsaturated hydraulic properties estimated with the tension infiltrometer and that this bias can preclude accurate estimation of spatial statistics. For this analysis, we develop Monte Carlo models to evaluate the effects of small, simple observation and inversion-model errors on estimated spatial statistics for the saturated hydraulic conductivity, K_s, and the single parameter for an exponential relative permeability, α. Observation errors consist of simple errors in infiltrometer flux-rates and applied tension at the infiltrometer source. Only one type of inversion-model error is modeled, a simple contact error. We generate spatially correlated random fields of α and K_s, simulate tension infiltrometer measurements with errors, and estimate α and K_s from the resulting tension infiltrometer data. When tension infiltrometer errors are due to observations only, spatial statistics of estimated hydraulic properties are most biased when the field mean α is high or the mean K_s is low, because flux rates are dominated by errors. When simple contact errors are included, the nature of the bias changes dramatically, and spatial statistics are most biased at low mean α. False cross-correlation between estimated parameters occurs because estimates of K_s depend on estimates of α and because both parameters are estimated from the same data.

Our results have broad implications for all other types of instruments used for characterizing spatial variability. All hydraulic properties are experimentally estimated using an instrument that observes the response of the hydrologic system to a transient or steady perturbation. Observed system states (e.g., pressure and flux-rates) are used in a mathematical inversion of the governing equations to infer the hydraulic property values. Observation and inversion-model errors lead to biased property estimates because most inversion models are non-linear. As a result, estimated hydraulic properties and their spatial statistics are biased. The extent of this bias depends on the non-linearity, the true values of the sampled hydraulic properties, and the nature of measurement and inversion-model errors present. Strong bias can produce or eliminate cross-correlation between parameters and preclude accurate estimation of the mean, variance, and variogram. The effects of observation and inversion-model error can be insidious, as hydraulic property estimates may appear reasonable and generate realistic-looking spatial statistics, which are, however, inaccurate and misleading. The geostatistical approaches used in spatial variability studies offer no formal approaches for detecting and treating measurement bias.

Robust field-estimation of hydraulic properties for spatial variability studies may not be possible with many current instruments and inversion models, because multiple parameters are estimated using a single, nonlinear model. In addition, bias in spatial statistics of estimated hydraulic properties is extremely sensitive to different inversion-model errors, and it is not possible to identify *a priori* all types of inversion-model error that may affect a particular property estimation method. Therefore, error analyses cannot be used to uniquely identify all material types or conditions under which a particular instrument or inversion model will perform best or to remove bias caused by measurement errors. For spatial variability studies, hydraulic properties are best estimated using direct measurements of the property or an essentially linear inversion model. If non-linear inversion-models are required, only one parameter should be estimated from a single model and data set.

Despite the difficulty and added cost, laboratory-estimated hydraulic properties may be preferable to field-estimated properties, because some properties are directly measured, measurement errors are smaller, and inversion-model errors can, to some extent, be controlled. However, this suggestion must be tested by studies of bias in estimated spatial statistics of laboratory-estimated hydraulic properties. Finally, the impact of bias in spatial statistics on stochastic models of flow and transport remains to be assessed.

ACKNOWLEDGEMENTS

This research was supported by the Department of Energy's Environmental Management Science Program (EMSP), through Grant No. DE-FG07-96ER14704. Tension infiltrometer experiments were performed at the Flow Visualization and Processes Laboratory at Sandia National Laboratories, and we thank Martha Whitaker for her help with this work. We also thank Sean McKenna and Jan Hendrickx for their reviews of an earlier version of this manuscript. We are especially grateful to Allan Gutjahr for his contributions in the early part of this work and reviews of early versions of this manuscript.

Sandia is a multiprogram laboratory operated by Sandia Corporation, a Lockheed Martin Company, for the United States Department of Energy under contract DE-AC04-94AL85000.

REFERENCES CITED

Ankeny, M. D., T. C. Kaspar, and R. Horton, Design for an automated tension infiltrometer, *Soil Sci. Soc. Am. J.*, *52*, 893-896, 1988.

Ankeny, M. D., M. Ahmed, T. C. Kaspar, and R. Horton, Simple field method for determining unsaturated hydraulic conductivity, *Soil Sci. Soc. Am. J.*, *55*, 467-470, 1991.

Beckie, R., Measurement scale, network sampling scale, and groundwater model parameters, *Water Resour. Res.*, *32(1)*, 65-76, 1996.

Bresler, E., Analysis of trickle irrigation systems with application to design problems, *Irrig. Sci.*, *1*, 3-17, 1978.

Brooks, R. H., and A. T. Corey, Hydraulic properties of porous media, *Hydrol. Pap. 3*, Colorado State University, Fort Collins, 1964.

Clothier, B. E., D. Scotter, and E. Harper, Three-dimensional infiltration and trickle irrigation, *Trans. Am. Soc. Agric. Eng.*, *28*, 497-501, 1985.

Davis, J.M., J.L. Wilson, and F.M. Phillips. A portable air-minipermeameter for in-situ field measurements, *Ground Water*, *32*, 258-266, 1994.

Deutsch, C. V., and A. G. Journel, GSLIB: *Geostatistical Software Library and User's Guide*, 2nd ed., Oxford University Press, New York, NY, 1992.

Doebelin, E. O., *Measurement Systems: Application & Design*, McGraw Hill, NY, NY, 1966.

DOE, Hydrogeologic data for existing excavations at the Area 5 Radioactive Waste Management site, Nevada Test Site, Nye County, Nevada, *DOE/NV/11432-40*, U.S. Department of Energy Nevada Operations Office, Las Vegas, NV, 1993.

Freeze, R. A., and J. A. Cherry, *Groundwater*, Prentice Hall, Englewood Cliffs, N.J., 1979.

Harter, T., and T. –C. Jim Yeh, Stochastic analysis of solute transport in heterogeneous, variably saturated soils, *Water Resour. Res., 32(6)*, 1585-1595, 1996.

Hussen A. A., and A. W. Warrick, Alternative analyses of hydraulic data from disc tension infiltrometers, *Water Resour. Res., 29(12)*, 4103-4108, 1993.

Indelman, P., D. Or, and Y. Rubin, Stochastic analysis of unsatured steady state flow through bounded heterogeneous formations, *Water Resour. Res., 29(4)*, 1141-1148, 1993.

Istok, J. D., D. O. Blout, L. Barker, K. R. Johnejack, and D. P. Hammermeister, Spatial variability in alluvium properties at a low-level nuclear waste site, *Soil Sci. Soc. Am. J., 58*, 1040-1051, 1994.

Jarvis, N. J., and I. Messing, Near-saturated hydraulic conductivity in soils of contrasting texture measured by tension infiltrometers, *Soil Sci. Soc. Am. J., 59*, 27-34, 1995.

Journel, A. G., and Ch. J. Huijbregts, *Mining Geostatistics*, Academic Press, Inc., New York, N.Y., 1978.

Kempthorne, O. and R. R. Allmaras, Errors and variability of observations, in A. Klute, Editor, *Methods of Soil Analysis, Part 1, Physical and Mineralogical Methods, 2nd Edition*, American Society of Agronomy and Soil Science Society of America, Madison, WI, 1-31, 1986.

Mandel, J., *The Statistical Analysis of Experimental Data*, Dover Publications, New York, NY, 1964.

Mantoglou, A. and L. W. Gelhar, Capillary tension head variance, mean soil moisture content, and effective specific soil moisture capacity of transient unsaturated flow in stratified soils, *Water Resour. Res., 23(1)*, 47-56, 1987a.

Mantoglou, A. and L. W. Gelhar, Effective hydraulic conductivities of transient unsaturated flow in stratified soils, *Water Resour. Res., 23(1)*, 57-67, 1987b.

Mohanty, B. P., M. D. Ankeny, R. Horton, and R. S. Kanwar, Spatial analysis of hydraulic conductivity measured using disc infiltrometers, *Water Resour. Res., 30(9)*, 2489-2498, 1994.

Parlange, J. –Y., and W. L. Hogarth, Steady state infiltration: Consequences of α dependent on moisture content, *Water Resour. Res., 21(8)*, 1283-1284, 1985.

Philip, J. R., Theory of infiltration, *Adv. Hydrosci., 5*, 215-296, 1969.

Polmann, D. J., D. McLaughlin, S. Luis, L. W. Gelhar, and R. Ababou, Stochastic modeling of large-scale flow in heterogeneous unsaturated soils, *Water Resour. Res., 27(7)*, 1447-1458, 1991.

Reynolds, W. D., and D. W. Elrick, Determination of hydraulic conductivity using a tension infiltrometer, *Soil Sci. Soc. Am. J., 55(3)*, 633-639, 1991.

Reynolds, W. D., and D. W. Elrick, A laboratory and numerical assessment of the Guelph permeameter method, *Soil Sci., 144*, 282-299, 1987.

Reynolds, W. D., and D. W. Elrick, In situ measurement of field saturated hydraulic conductivity, sorptivity, and the α-parameter using the Guelph permeameter, *Soil Sci.*, *140*, 292-302, 1987.

Robin, M. J. L., A. L. Gutjahr, E. A. Sudicky, and J. L. Wilson, Cross-correlated random field generation with the direct Fourier transform method, *Water Resour. Res.*, *29(7)*, 2385-2397, 1993.

Russo, D., Design of an optimal sampling network for estimating the variogram, *Soil Sci. Soc. Am. J.*, *48*, 708-716, 1984.

Russo, D., Stochastic analysis of the velocity covariance and the displacement covariance tensors in partially saturated heterogeneous anisotropic porous formations, *Water Resour. Res.*, *31(7)*, 1647-1658, 1995.

Russo, D., and W. A. Jury, A theoretical study of the estimation of the correlation scale in spatially variable fields: 1. Stationary fields, *Water Resour. Res.*, *23(7)*, 1259-1269, 1987a.

Russo, D., and W. A. Jury, A theoretical study of the estimation of the correlation scale in spatially variable fields: 1. Nonstationary fields, *Water Resour. Res.*, *23(7)*, 1269-1279, 1987b.

Russo, D., and M. Bouton, Statistical analysis of spatial variability in unsaturated flow parameters, *Water Resour. Res.*, *28(7)*, 1911-1925, 1992.

Russo, D., I. Russo, and A. Laufer, On the spatial variability of parameters of the unsaturated hydraulic conductivity, *Water Resour. Res.*, *33(5)*, 947-956, 1997.

Shouse, P. J., and B. P. Mohanty, Scaling of near-saturated hydraulic conductivity measured using disc infiltrometers, *Water Resour. Res.*, *34(5)*, 1195-1205, 1998.

Simunek, J, O. Wendroth, M. T. van Genuchten, Estimating unsaturated soil hydraulic properties from laboratory tension disc infiltrometer experiments, *Water Resour. Res.*, *35(10)*, 2965-2979, 1999.

Simunek, J, and M. T. van Genuchten, Estimating unsaturated soil hydraulic properties from tension disc infiltrometer data by numerical inversion, *Water Resour. Res.*, *32(9)*, 2683-2696, 1996.

Soil Measurement Systems, *Tension Infiltrometer Users Manual*, Soil Measurement Systems, Tucson, AZ, 1992.

van Genuchten, M. Th., A closed–form equation for predicting the hydraulic conductivity of unsaturated soils, *Soil Sci. Soc. Am. J.*, *44*, 892-898, 1980.

Warrick, A. W., and D. E. Myers, Optimization of sampling locations for variogram calculations, *Water Resour. Res.*, *23(3)*, 496-500, 1987.

Weast, R. C., ed., *Handbook of Chemistry and Physics*, 53 rd edition., CRC Press, Cleveland, OH, 1972.

White, I., and M. J. Sully, On the variability and use of the hydraulic conductivity alpha parameter in stochastic treatments of unsaturated flow, *Water Resour. Res.*, *28(1)*, 209-213, 1992.

Wooding, R. A., Steady infiltration from a shallow circular pond, *Water Resour. Res.*, *4(6)*, 1259-1273, 1968.

Wu, L., L. Pan, M. J. Roberson, and P. J. Shouse, Numerical evaluation of ring-infiltrometers under various soil conditions, *Soil Sci.*, *162*, 771-777, 1997.

Yeh, T. –C. Jim, L. W. Gelhar, and A. L. Gutjahr, Stochastic analysis of unsaturated flow in heterogeneous soils: 1. Statistically isotropic media, *Water Resour. Res., 21(4)*, 447-456, 1985a.

Yeh, T. –C. Jim, L. W. Gelhar, and A. L. Gutjahr, Stochastic analysis of unsaturated flow in heterogeneous soils: 2. Statistically isotropic media with variable α, *Water Resour. Res., 21(4)*, 457-464, 1985b.

Yeh, T. –C. Jim, L. W. Gelhar, and A. L. Gutjahr, Stochastic analysis of unsaturated flow in heterogeneous soils: 3. Observations and applications, *Water Resour. Res., 21(4)*, 465-471, 1985c.

Zhang, D. Z., T. C. Wallstrom, and C. L. Winter, Stochastic analysis of steady-state unsaturated flow in heterogeneous media: Comparison of the Brooks-Corey and Gardner-Russo models, *Water Resour. Res., 34(6)*, 1437-1449, 1998.

LIST OF FIGURES

Figure 1. Schematic of the tension infiltrometer. The base plate (on the right) is in contact with the sampled medium.

Figure 2. Fraction of points rejected as a function of parameter space with a) observation error and b) also with contact error.

Figure 3. The ratio $\hat{\alpha}^G / \alpha^G$ with a) observation error and b) also with contact error. The $\hat{K}_s^G / K_s^G$ with c) observation error and d) also with contact error. The most accurate region, relative error between 0.95 and 1.05, is shaded.

Figure 4. The variance of $\hat{\alpha}$ shown as a ratio $(\sigma^2_{\ln(\hat{\alpha})} / \sigma^2_{\ln(\alpha)})$ with a) observation error only and b) also with contact error. The variance of $\hat{K}_s$ shown as a ratio $(\sigma^2_{\ln(\hat{K}_s)} / \sigma^2_{\ln(K_s)})$ with c) observation error and d) also with contact error. The most accurate region, relative error between 0.95 and 1.05, is shaded.

Figure 5. Variogram model parameters for ln($\hat{\alpha}$),shown as a ratio of "estimated"/"true": a) model variance with measurement errors only, b) correlation length with measurement error only, c) model variance with contact error, and d) correlation length with contact error. The most accurate region, ratio value between 0.95 and 1.05, is shaded. Regions equal to zero are patterned indicating nugget variograms.

Figure 6. Variogram model parameters for $\ln(\hat{K}_s)$, shown as a ratio of "estimated"/"true": a) model variance with measurement errors only, b) correlation length with measurement error only, c) model variance with contact error, and d) correlation length with contact error. The most accurate region, ratio value between 0.95 and 1.05, is shaded. Regions equal to zero are patterned.

Figure 7. Correlation coefficients for $\ln(\hat{\alpha})$ and $\ln(\hat{K}_s)$ as a function of parameter space: a) with measurement error only and b) also with contact error. Regions equal to zero are patterned.

Figure 1

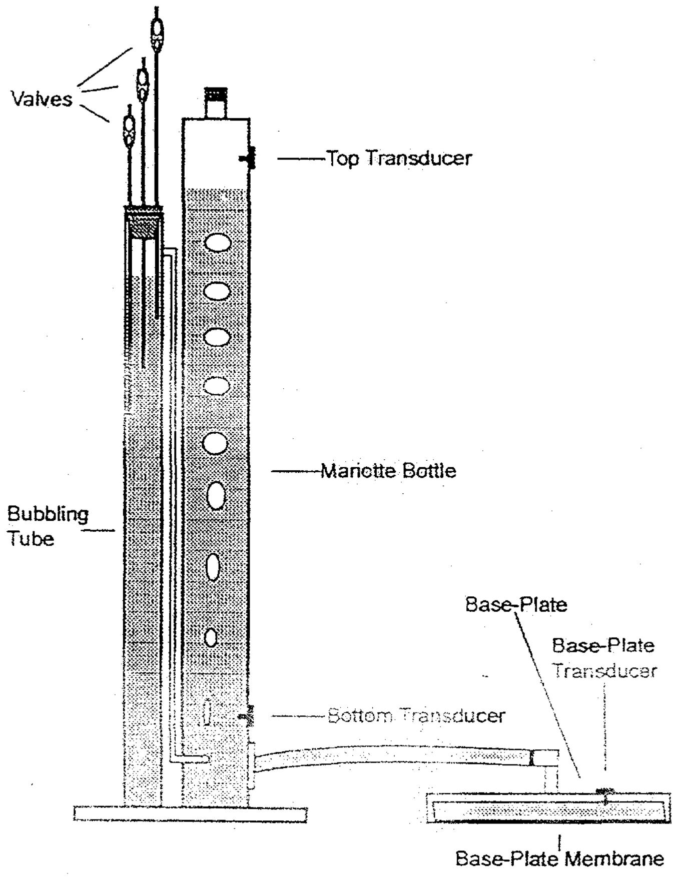
Valves
Top Transducer
Mariotte Bottle
Bubbling Tube
Base-Plate
Base-Plate Transducer
Bottom Transducer
Base-Plate Membrane

Figure 2

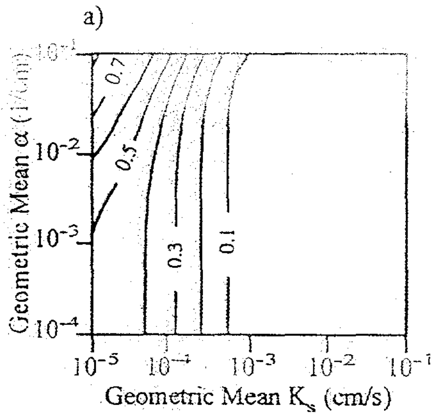
a)
0.7
0.5
0.3
0.1
Geometric Mean α (1/cm)
10⁻¹
10⁻²
10⁻³
10⁻⁴
10⁻⁵
10⁻⁴
10⁻³
10⁻²
10⁻¹
Geometric Mean K_s (cm/s)
b)
0.6
0.5
0.4
0.3
0.2
0.1
Geometric Mean α (1/cm)
Geometric Mean K_s (cm/s)

Figure 3

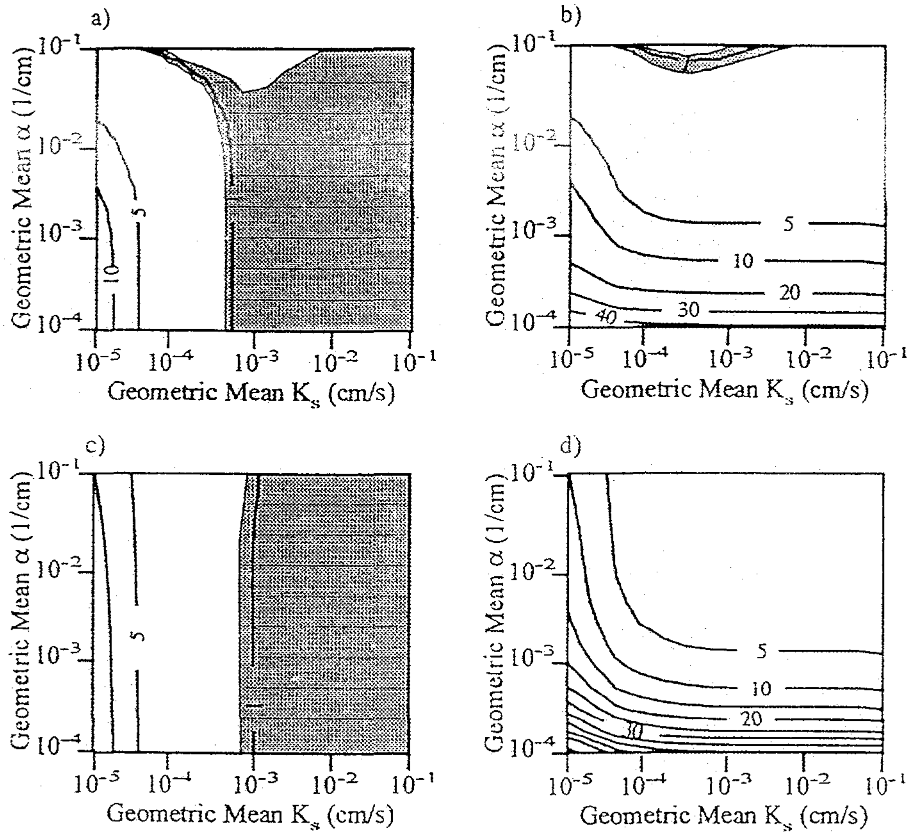
a)
b)
c)
d)
Geometric Mean α (1/cm)
Geometric Mean K_s (cm/s)
10^{-1}
10^{-2}
10^{-3}
10^{-4}
10^{-5}
5
10
20
30
40

Figure 4

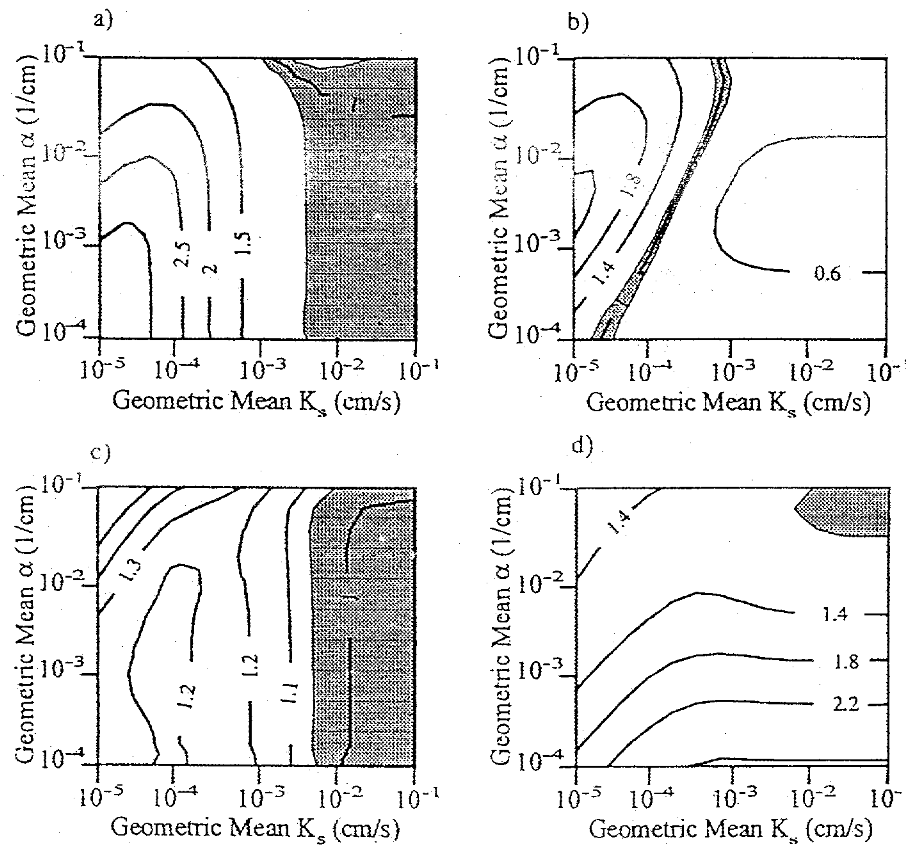

a)
b)
c)
d)
Geometric Mean α (1/cm)
Geometric Mean K_s (cm/s)
10^-1
10^-2
10^-3
10^-4
10^-5
2.5
2
1.5
1.8
1.4
0.6
1.3
1.2
1.1
2.2

Figure 5

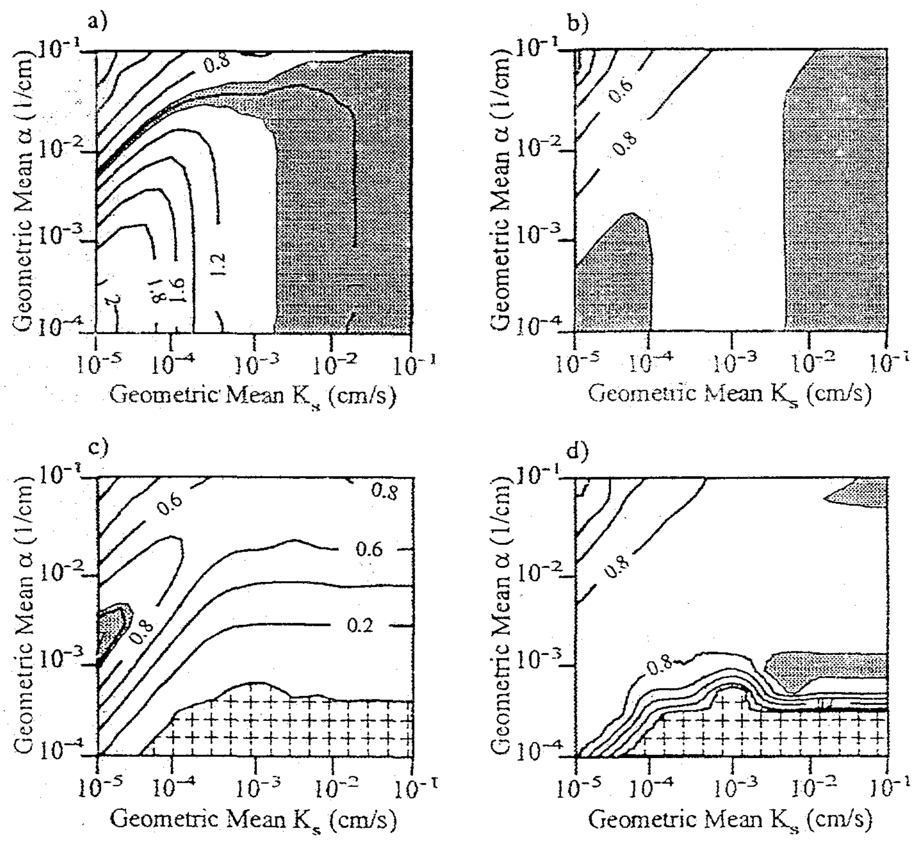
a)
b)
c)
d)
Geometric Mean α (1/cm)
Geometric Mean K_s (cm/s)
10^{-1}
10^{-2}
10^{-3}
10^{-4}
10^{-5}
0.8
1.2
1.6
1.8
2
0.6
0.2

Figure 6

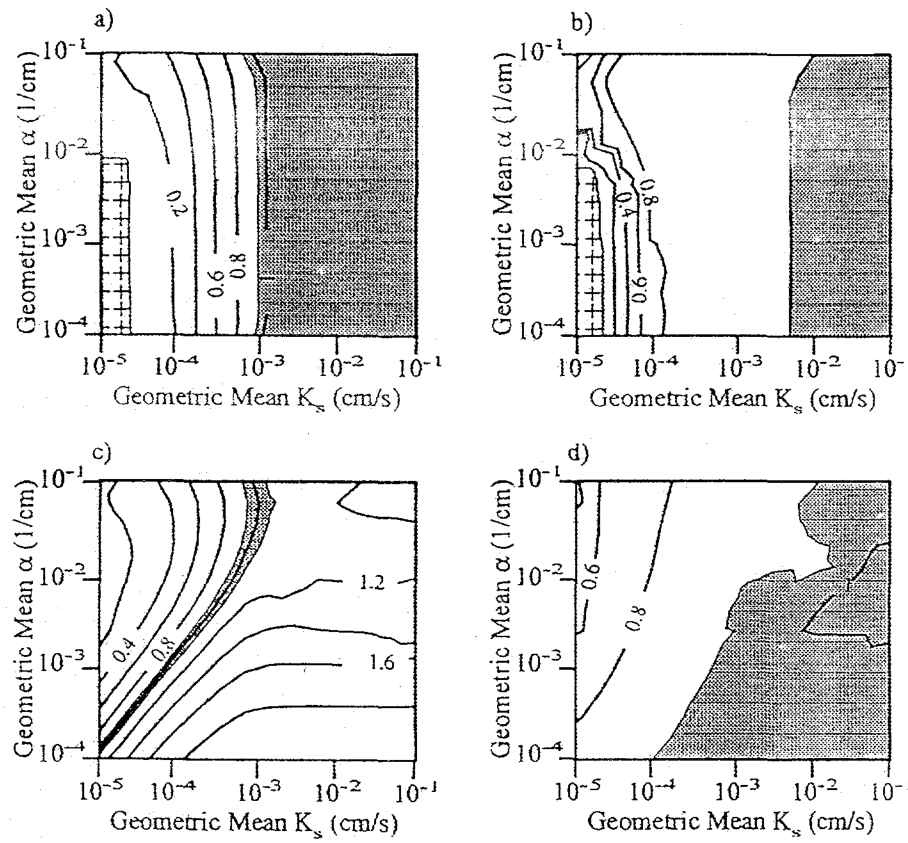
a)
b)
c)
d)
Geometric Mean α (1/cm)
Geometric Mean K_s (cm/s)
10^-1
10^-2
10^-3
10^-4
10^-5
0.2
0.4
0.6
0.8
1.2
1.6

Figure 7

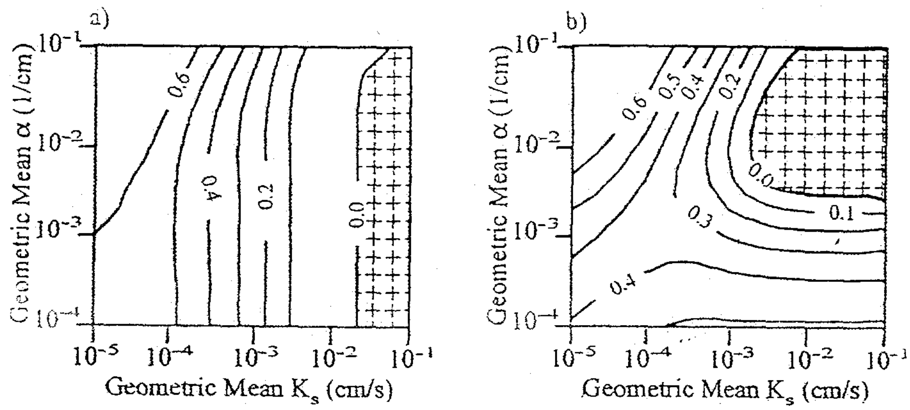
a)
Geometric Mean α (1/cm)
10^{-1}
10^{-2}
10^{-3}
10^{-4}
0.6
0.4
0.2
0.0
10^{-5} 10^{-4} 10^{-3} 10^{-2} 10^{-1}
Geometric Mean K_s (cm/s)
b)
Geometric Mean α (1/cm)
10^{-1}
10^{-2}
10^{-3}
10^{-4}
0.6
0.5
0.4
0.2
0.0
0.1
0.3
0.4
10^{-5} 10^{-4} 10^{-3} 10^{-2} 10^{-1}
Geometric Mean K_s (cm/s)